

1                   **Force-induced changes of PilY1 drive surface sensing by**  
2                                   ***Pseudomonas aeruginosa***  
3  
4

5 Shanice S. Webster<sup>1</sup>, Marion Mathelié-Guinlet<sup>2</sup>, Andreia F. Verissimo<sup>3</sup>, Daniel Schultz<sup>1</sup>, Albertus  
6 Viljoen<sup>2</sup>, Calvin K. Lee<sup>4,5,6</sup>, William C. Schmidt<sup>4,5,6</sup>, Gerard C. L. Wong<sup>4,5,6</sup>, Yves F. Dufrene<sup>2</sup>,  
7 George A. O'Toole<sup>1,\*</sup>  
8

9 <sup>1</sup>Department of Microbiology and Immunology, Geisel School of Medicine at Dartmouth,  
10 Hanover NH 03755, USA

11 <sup>2</sup>Louvain Institute of Biomolecular Science and Technology, Université Catholique de  
12 Louvain, Croix du Sud, 4-5, bte L7.07.07, B-1348 Louvain-la-Neuve, Belgium

13  
14 <sup>3</sup>Institute for Biomolecular Targeting (bioMT), Geisel School of Medicine at Dartmouth,  
15 Hanover NH 03755, USA

16  
17 <sup>4</sup>Department of Bioengineering, University of California Los Angeles, CA 90095

18  
19 <sup>5</sup>Department of Chemistry and Biochemistry, University of California Los Angeles, CA 90095

20  
21 <sup>6</sup>California NanoSystems Institute, University of California Los Angeles, CA 90095  
22

23  
24 **\*Corresponding author:**

25 George A. O'Toole

26 Dept. of Microbiology & Immunology

27 Rm 202 Remsen Building

28 66 College Street

29 Geisel School of Medicine at Dartmouth

30 Hanover, NH 03755

31 Phone: (603) 650-1248

32 [georgeo@dartmouth.edu](mailto:georgeo@dartmouth.edu)  
33

34 Key Words: type 4 pili, force, PilY1, von Willebrand A domain, surface sensing, c-di-GMP  
35  
36  
37  
38  
39

## 40 **Abstract**

41  
42 During biofilm formation, the opportunistic pathogen *Pseudomonas aeruginosa* uses its type IV  
43 pili (TFP) to sense a surface, eliciting increased second messenger production and regulating  
44 target pathways required to adapt to a surface lifestyle. The mechanisms whereby TFP detect  
45 surface contact is still poorly understood, although mechanosensing is often invoked with little  
46 data supporting this claim. Using a combination of molecular genetics and single cell analysis,  
47 with biophysical, biochemical and genomics techniques we show that force-induced changes  
48 mediated by the von Willebrand A (vWA) domain-containing, TFP tip-associated protein PilY1  
49 are required for surface sensing. Atomic force microscopy shows that PilY1 can undergo force-  
50 induced, sustained conformational changes akin to those observed for mechanosensitive  
51 proteins like titin. We show that mutation of a single cysteine residue in the vWA domain results  
52 in modestly lower surface adhesion forces, increased nanospring-like properties, as well as  
53 reduced c-di-GMP signaling and biofilm formation. Mutating this cysteine has allowed us to  
54 genetically separate TFP function in twitching from surface sensing signaling. The conservation  
55 of this Cys residue in all *P. aeruginosa* PA14 strains, and its absence in the ~720 sequenced  
56 strains of *P. aeruginosa* PAO1, could contribute to explaining the observed differences in  
57 surface colonization strategies observed for PA14 versus PAO1.

58

## 59 **Importance**

60 Most bacteria live on abiotic and biotic surfaces in surface-attached communities known as  
61 biofilms. Surface sensing and increased levels of the second messenger molecule c-di-GMP are  
62 crucial to the transition from planktonic to biofilm growth. The mechanism(s) underlying TFP-  
63 mediated surface detection that triggers this c-di-GMP signaling cascade are unclear. Here, we  
64 provide a key insight into this question: we show that the eukaryotic-like, vWA domain of the TFP  
65 tip-associated protein PilY1 responds to mechanical force, which in turn drives production of a

66 key second messenger needed to regulate surface behaviors. Our studies highlight a potential  
67 mechanism that could account for differing surface colonization strategies.

68  
69 **Introduction**

70  
71 *Pseudomonas aeruginosa* is a ubiquitously distributed opportunistic pathogen that  
72 encounters mechanical forces during surface sensing – a crucial first step for biofilm formation.  
73 The type four pili (TFP) motility appendage is integral to surface sensing and is thought to  
74 transduce a force-induced signal to the cell interior by detecting the resistance to retraction  
75 when cells are surface engaged [1], activating the production of cAMP and c-di-GMP, and  
76 regulating target genes that control biofilm formation [2-4]. While the importance of the TFP and  
77 its tip associated protein, PilY1, in surface sensing has been proposed, direct evidence of how  
78 the TFP/PilY1 sense the surface is lacking. Indeed, much of the supporting evidence of a role  
79 for this appendage as a key surface sensor is deductive, or alternatively, rely on biological  
80 responses or phenotypic changes that are observed during the switch from planktonic to  
81 surface-attached growth. In this study, we thus take a multi-disciplinary approach to investigate  
82 the mechanism whereby the TFP via the tip-associated protein, PilY1, is directly involved in  
83 surface sensing.

84 PilY1 is part of the priming complex together with the minor pilins that facilitate  
85 incorporation of the PilA subunits into the base of the growing pilus fiber during elongation [5, 6].  
86 During polymerization, the minor pilins and PilY1 are pushed to the tip of the growing pilus.  
87 PilY1 has a C-terminal domain that resembles PilC from *Neisseria gonorrhoea* and a N-terminal  
88 von Willebrand A (vWA) domain (Fig. 1A) that is structurally similar to the A2 domain of the  
89 human von Willebrand factor (vWF), a force sensing glycoprotein important in stopping bleeding  
90 [4]. The vWA domain of PilY1 has the classical Rossman fold – central beta sheets surrounded  
91 by amphipathic alpha helices [7] – and a perfectly conserved metal ion dependent adhesion site  
92 (MIDAS) containing the conserved DxSxS...T...F motif [8]. vWA domains have been reported in

93 TFP-associated proteins from other organisms. For example, the vWA domain of the major pilin  
94 in *Streptococcus agalactiae* is essential for adhesion [9] and the MIDAS motif in the vWA  
95 domain of the major pilin in *Streptococcus sanguinis* has recently been shown to be important in  
96 binding to eukaryotic cells [10]. Like the vWF [11], the vWA domain of *P. aeruginosa* PA14 PilY1  
97 protein also has a high number of cysteine residues; seven out of the 11 cysteines in PilY1 are  
98 in its vWA domain. Interestingly, during vascular damage, when exposed to high shear forces  
99 due to blood flow, the vWF transitions from a globular to a stretched conformation [12, 13]. This  
100 transition is thought to be mediated by a disulfide bond switch exposing specific sites that allow  
101 platelets to bind [14-16]. Thus, vWF cysteine residues, depending on their redox state, are key  
102 to force sensing, a property that could be hypothesized for cysteine residues in the vWA of  
103 PilY1.

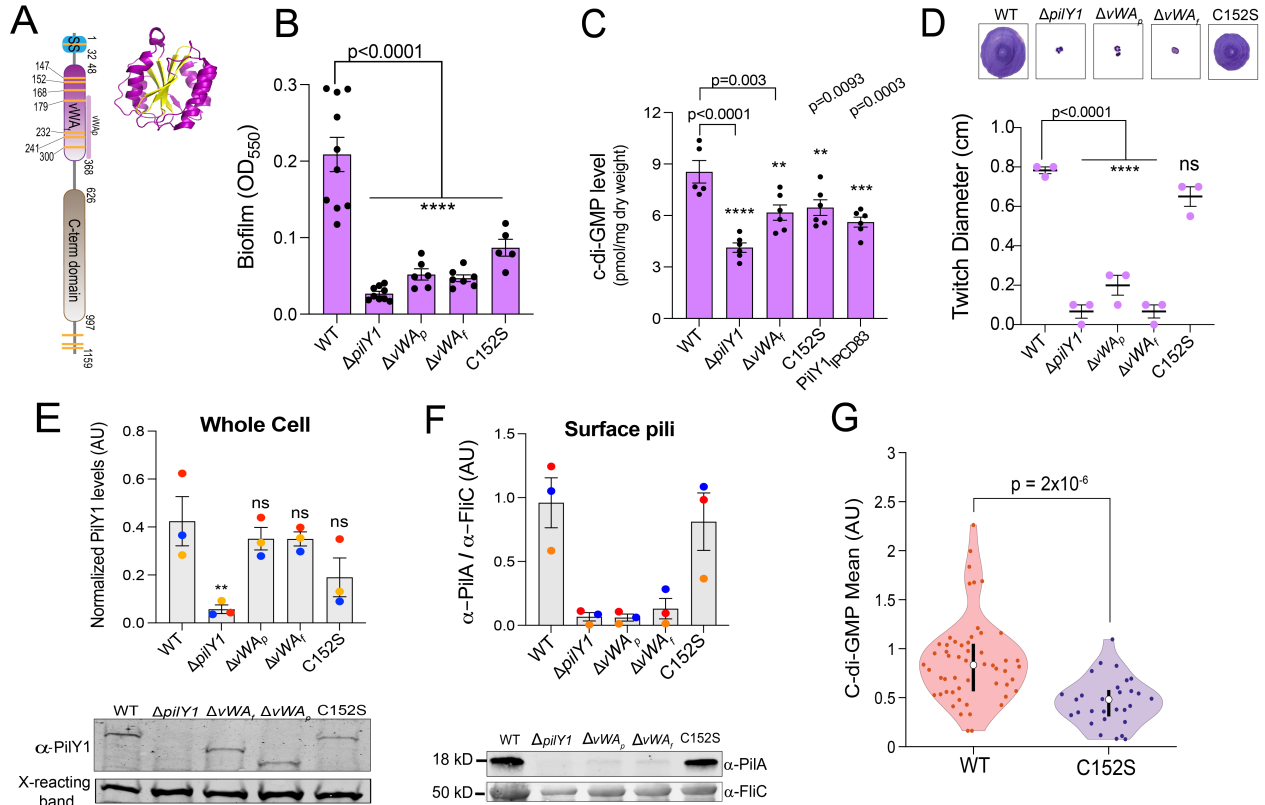
104         Although PilY1 is known to be important in responding to shear forces and in increasing  
105 c-di-GMP levels [3, 17, 18], the precise role of its vWA domain in surface sensing and c-di-GMP  
106 signaling is unclear. Our previous genetic studies show that PilY1 and the vWA domain are  
107 important for surface-dependent stimulation of c-di-GMP production [3, 18]. These studies also  
108 showed that while the C-terminal domain of PilY1 was dispensable for surface-dependent c-di-  
109 GMP production, strains with mutations in the vWA domain failed to regulate c-di-GMP levels  
110 and c-di-GMP-related behaviors [18]. Additionally, deletion of the vWA domain is shown to lock  
111 PilY1 in a constitutively active signaling conformation that induces virulence independent of  
112 surface attachment [4], suggesting multiple roles for the vWA domain in the surface-attached  
113 biology of *P. aeruginosa*.

114         Recent cryo-electron tomography studies show the vWA domain of PilY1 to be situated at  
115 the very tip of the pilus fiber [5] indicating that this domain is likely in immediate contact with the  
116 surface and therefore could be directly engaged in surface sensing. Based on the similarities  
117 between the human vWF and the vWA domain of PilY1, and its importance in downstream c-di-

118 GMP signaling, we hypothesized that force-induced conformational changes originating from the  
119 vWA domain of PilY1 are mediated by conserved cysteine residues within this putative  
120 mechanosensing domain, and together these features of PilY1 are critical for surface sensing.  
121 We explore these hypotheses here.

## 122 123 **Results**

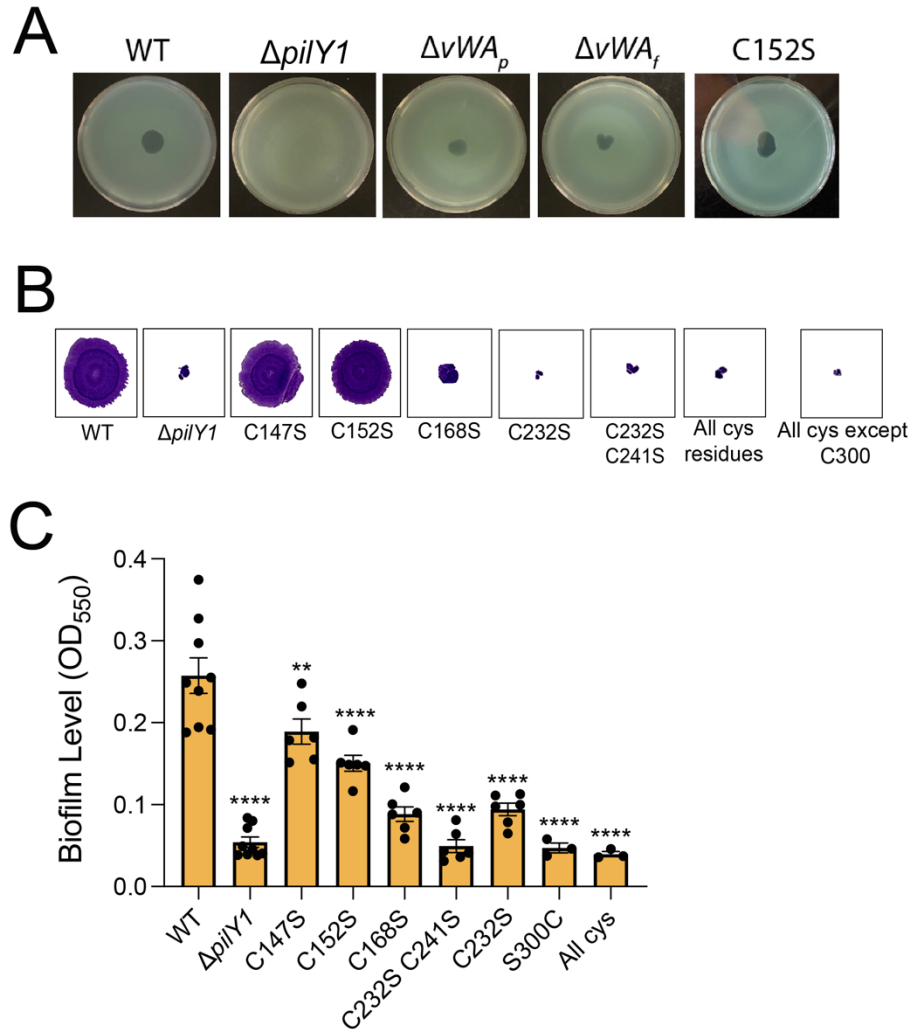
124 **The von Willebrand A (vWA) domain of PilY1 regulates c-di-GMP levels and biofilm**  
125 **formation.** To address the role of the vWA domain of PilY1 in surface sensing and c-di-GMP  
126 signaling, we made chromosomal deletions that removed a part ( $\Delta vWA_p$ ) or the full ( $\Delta vWA_f$ , **Fig.**  
127 **1A**) vWA domain, then performed static biofilm assays and measured global levels of c-di-GMP  
128 (**Fig. 1B** and **C**). Our bulk assays show that both the  $\Delta vWA_p$  and  $\Delta vWA_f$  variants resulted in a  
129 significant decrease in biofilm formation and reduction in global c-di-GMP levels (as seen for the  
130  $\Delta vWA_f$  variant) as compared to WT. These vWA variants also resulted in no twitching motility  
131 (**Fig. 1D**). To confirm these twitch phenotypes, another more sensitive assay was used based  
132 on the lysis of the host cells *P. aeruginosa* PA14 by the lytic DMS3<sub>vir</sub> phage, which specifically  
133 targets the TFP and also requires retraction of surface-expressed pili for infection [19]. Strains  
134 carrying the  $\Delta vWA_p$  and  $\Delta vWA_f$  variants showed partial zones of clearing in a phage plaquing  
135 assays (**Fig. S1A**), indicating that these strains retained some TFP function. To further ensure  
136 that the decrease in biofilm formation and reduced c-di-GMP levels were not due to protein  
137 instability, we examined steady state levels of the vWA variants in whole cell extracts. Both the  
138  $\Delta vWA_p$  and  $\Delta vWA_f$  PilY1 variants were stable and showed a non-significant reduction in whole  
139 cell levels as compared to WT (**Fig. 1E**). However, little surface pili could be detected in the  
140 strains expressing the  $\Delta vWA_p$  and  $\Delta vWA_f$  variants (**Fig. 1F**), which likely explains the lack of full  
141 pilus function observed in the twitch assays (**Fig. 1D**). The presence of plaques (**Fig. S1A**),  
142 however, indicates that there are some surface pili, a finding consistent with our Western blots  
143 (**Fig. 1F**).



144  
145  
146  
147  
148  
149  
150  
151  
152  
153  
154  
155  
156  
157  
158  
159  
160  
161  
162  
163  
164  
165  
166  
167  
168  
169  
170  
171  
172  
173

**Figure 1. The von Willebrand A (vWA) domain and Cys152 residue of PilY1 are important for regulating c-di-GMP levels and biofilm formation.** **A.** Schematic showing domain organization of the PilY1 protein. The signal sequence (SS – blue, amino acids 1-32), vWA domain (pink, amino acids 48-368) and C-terminal domain (brown, amino acids 626-997) are highlighted. vWAp (amino acids S168-S365) denotes a portion of the vWA domain that is deleted in a mutant analyzed in the subsequent panels. Yellow stripes represent the cysteines residues present in the protein. The vWA domain contains seven of the 11 cysteine residues present in the full length PilY1 protein with the SS and the C-terminal region having one and three cysteine residues, respectively. Inset: Ribbon diagram showing the vWF A2 domain (PDB 3GXB). The domain shows a classical Rossmann fold [7], comprised of central  $\beta$ -sheets (yellow) surrounded by  $\alpha$ -helices (purple). **B.** Biofilm formation measured at OD<sub>550</sub> for WT, the  $\Delta pilY1$  deletion mutant, the vWA variants, and the Cys152S mutant in a static 96 well biofilm assay performed in M8 medium salts plus supplements (see Materials and Methods) and incubated at 37 °C for 24 h. vWAp (amino acids 178-365, see panel A) and vWAf indicate a partial and full deletion (amino acids 48-368) of the vWA domain, respectively. Data are from at least five biological replates each with eight technical replicates. **C.** Quantification of global c-di-GMP levels by mass spectrometry for WT and the indicated mutants shown in picomole per milligram dry weight. Cells were grown on 0.5% agar plates prepared with M8 medium salts plus supplements, then scraped from the plates after incubation for 37 °C for 14-16 h. Data are from six biological replicates each with two technical replicates. **D.** Twitch diameter (cm) for WT and the indicated mutants measured after inoculating LB plates from overnight cultures, then incubating the plates for 24 h at 37 °C plus an additional day at room temperature. Representative images of twitch zones are shown above the graph. Data are from three biological replicates. **E.** Quantification of normalized PilY1 protein levels in whole cell (in arbitrary units (AU)) for WT and the indicated mutants. Cells were sub-cultured from an overnight culture and grown to mid-log phase in M8 medium salts plus supplements and normalized to the same OD<sub>600</sub> value. Protein levels in whole cell extracts are normalized to a cross-reacting band at ~60 kDa, which is used as an additional loading control. The Cys152S mutant shows a modest but not significant reduction in level in whole cell extracts. A representative Western blot image for PilY1 and the cross-reacting band are shown below the graph. **F.** Quantification of normalized surface pili levels. PilA (~18 kDa) protein levels are used as a surrogate for surface pili levels, which are normalized to levels of the flagellar protein, FliC (~50 kDa). A representative Western blot is shown below the graph. All Western blot data are from three biological replicates in three independent experiments. Dots with the same color represent the same biological replicate; different colors indicate different biological replicates. p values:  $p \leq 0.05$ , ns, not significant. All error bars in Figure 1 are

174 standard error of the mean (SEM) and statistical significance was determined by one-way ANOVA and a Dunnett's  
 175 post-hoc test, p-values:  $p \leq **** 0.0001$ ,  $p \leq *** 0.001$ ,  $p \leq ** 0.01$ , ns, not significant. **G.** Violin plots showing the  
 176 mean c-di-GMP of the WT strain and a strain expressing the vWA-Cys152S PilY1 variant during early biofilm  
 177 formation. c-di-GMP level was quantified from GFP intensity determined on a cell-by-cell basis in a microfluidic  
 178 chamber carrying the  $P_{cdrA}$ -GFP construct, which is a reporter of c-di-GMP levels. NOTE: The WT data shown here  
 179 was first reported in a previous publication [20]; each strain analyses is done independently, in the same system and  
 180 medium, with the same microscope at identical settings and processed as reported [20]. Given that each analysis is  
 181 independent but performed identically, we can compare data from previous studies. Each data point represents one  
 182 tracked cell through an entire division cycle. Statistical significance was determined using the Kruskal-Wallis test,  $p$   
 183  $= 2 \times 10^{-6}$ .



219 **Figure S1. Partial functionality of vWA variants and phenotypic analysis of other cysteine vWA mutants. A.**  
 220 Plaque assay with phage DMS3<sub>vir</sub> versus the WT and the indicated mutants as hosts. Zones of clearing shown for  
 221 WT and the strain expressing the vWA-Cys152S mutant protein are similar, which indicates a similar degree of TFP  
 222 function. The  $\Delta pilY1$  mutant serves as the negative control. **B.** Representative images of twitch zones stained with  
 223 crystal violet shown for WT, the  $\Delta pilY1$  or strains expressing PilY1 variants with point mutations in the Cys  
 224 residues in the vWA domain following incubation at 37 °C for 24 h plus one additional day at room temperature.  
 225 Twitching serves as a measure of TFP function. **C.** Biofilm level measured at OD<sub>550</sub> for WT and the mutants shown  
 226 in panel B using the 96 well static biofilm assay after 24 hrs at 37 °C, as described in the Materials and Methods.



227 **The Cys152 residue of the vWA domain is important for promoting biofilm formation and**  
228 **regulating c-di-GMP levels.** Multimerization and conformational changes required for function  
229 in blood clotting by the human vWF are mediated by cysteine residues [15, 16, 21]. Shear  
230 forces due to blood flow during vascular damage have been shown to induce disulfide bond  
231 cleavage, which results in the protein adopting a new, stretched conformation [21, 22]. Inspired  
232 by these studies and the high number of cysteines in the vWA domain of PilY1 (**Fig. 1A**), we  
233 hypothesized that one or more cysteines in the vWA domain of PilY1 might be important for  
234 mediating conformational changes in PilY1 and/or the pilus fiber that could in turn impact  
235 surface sensing and downstream c-di-GMP signaling. To test this hypothesis, we performed  
236 targeted mutagenesis of the cysteine residues in the vWA domain of PilY1 with the aim of  
237 identifying one or more of these residues that impact biofilm formation but still retain TFP  
238 function as assessed by twitching assays. In all cases, the mutations were introduced into the  
239 chromosomal copy of the *pilY1* gene, thus the mutants were expressed under the native *pilY1*  
240 promoter and in their native chromosomal context. Of the seven individual and combination  
241 cysteine residues mutated, five resulted in decreased biofilm formation but no twitching motility  
242 (**Fig. S1B and S1C**). However, two residues, when mutated (vWA-C147S and vWA-Cys152S)  
243 displayed decreased biofilm formation but retained twitching motility (**Fig. 1B, D and Fig. S1B**).  
244 Because the vWA-Cys152S mutation yielded the stronger biofilm phenotype, we focused on this  
245 mutant for all subsequent analyses.

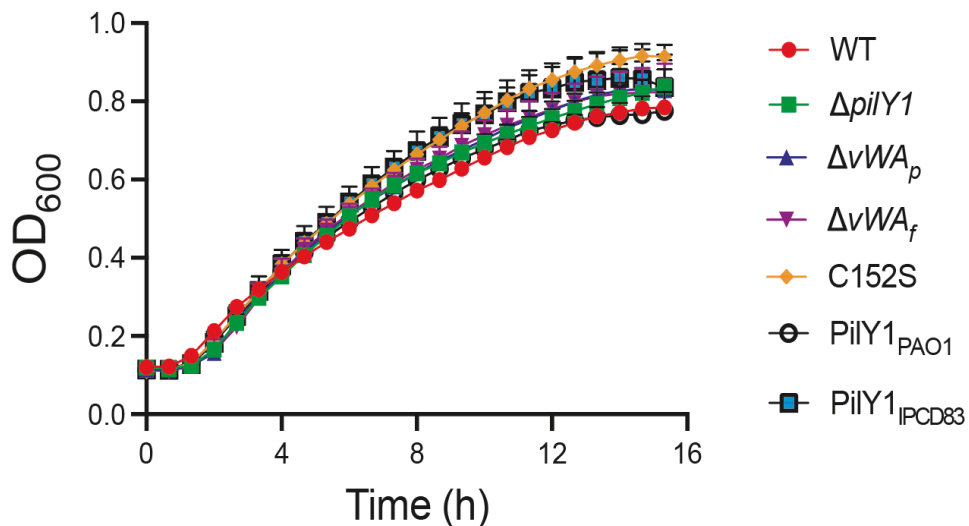
246 We next measured c-di-GMP levels globally and on a cell-by-cell basis for the strain  
247 expressing the vWA-Cys152S variant. Compared to WT, the vWA-Cys152S mutant showed  
248 significantly reduced levels of c-di-GMP based on bulk measurements of cell extracts and on a  
249 single-cell basis (**Fig. 1C and Fig. 1G**, respectively). Note: the WT data shown in the single cell  
250 data (**Fig. 1G**) was first reported in a previous publication [20]. Analyses of WT and vWA-  
251 Cys152S were done independently, in the same system and medium, analyzed with the same



252 microscope at identical settings and processed as reported [20]. Given that each investigation is  
253 independent but performed identically, it allows us to compare data from this previous report.

254         Given the similar levels of twitching motility for the strain carrying the vWA-Cys152S  
255 mutant and the WT, we predicted that this point mutation would yield a stable PilY1 protein.  
256 Western blot studies of whole cells showed that the vWA-Cys152S variant is stable and shows  
257 a modest but non-significant reduction in protein levels as compared to WT PilY1 (**Fig. 1E**).  
258 Additionally, surface pili levels for the strain expressing the vWA-Cys152S mutant protein are  
259 comparable to WT (**Fig. 1F**). These results are consistent with the vWA-Cys152S mutant  
260 showing similar levels of twitching motility (**Fig. 1D**) and plaque formation (**Fig. S1A**) compared  
261 to WT. Of note, none of the observed phenotypes are due to differences in growth rates as the  
262 vWA-Cys152S strain along with all vWA mutants used in this study have the same growth  
263 kinetics as WT (**Fig. S2**).

264



265

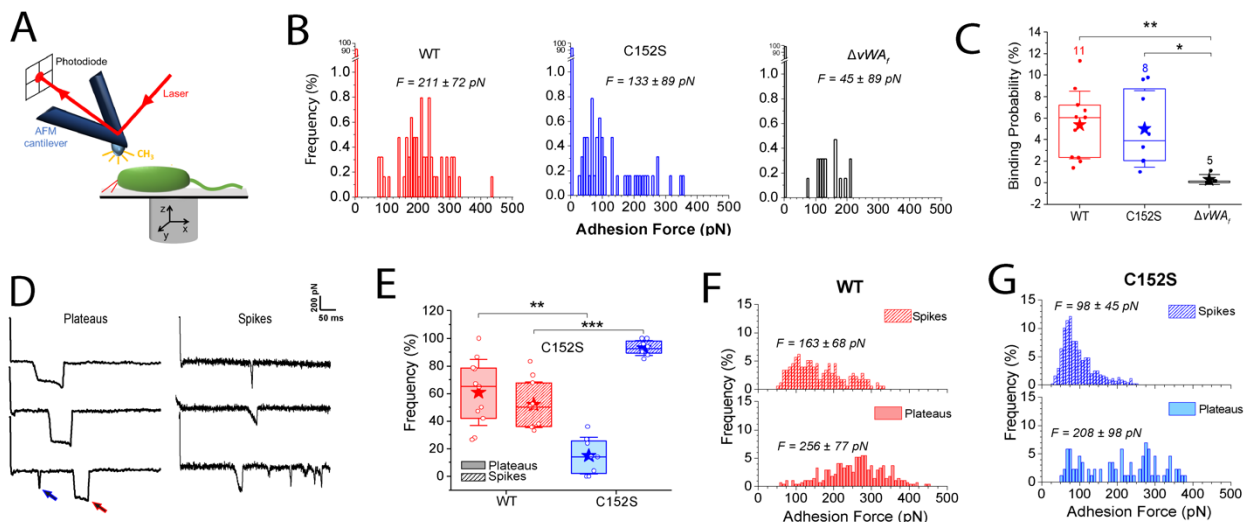
266 **Figure S2. Growth curves for WT and the strains expressing the PilY1 variants.** Growth assays were performed  
267 in M8 minimal salts medium supplemented with casamino acids, glucose and magnesium sulfate. This medium was  
268 also used for all macroscopic biofilm assays, c-di-GMP measurements, plaquing assays and AFM studies. The data  
269 are from three biological replicates each with two technical replicates. There is no significant difference among the  
270 growth kinetics of each strain. Error bars show SEM and statistical significance was determined at each time point  
271 using one-way analysis of variance (ANOVA) using multiple comparisons test.

272           **The vWA-Cys152S variant of PilY1 is associated with lower surface adhesion**  
273 **forces and altered force-induced behaviors.** In light of the key role of the vWA domain in  
274 biofilm formation and c-di-GMP regulation, we next sought to investigate the different surface  
275 adhesion behaviors of *P. aeruginosa* strains expressing WT PilY1, or the PilY1 variants with the  
276  $\Delta vWA_f$  or the vWA-Cys152S mutations. To this end, we used atomic force microscopy (AFM), a  
277 powerful multifunctional technique that has been instrumental in deciphering the adhesion and  
278 nanomechanical properties of bacterial pili, at the single-cell and single-molecule levels [23-25].  
279 More specifically, we recorded the force experienced by a hydrophobic AFM tip when probed  
280 against the TFP of surface engaged bacterial cells as a function of the tip-sample surface  
281 distance (**Fig. 2A**). From the resulting force-distance curves, binding probability and adhesion  
282 forces were determined on multiple living cells. As illustrated in the representative force  
283 histograms (**Fig. 2B**), the vWA-Cys152S mutant showed a lower adhesion force than WT cells  
284 ( $F = 133 \pm 89$  pN and  $211 \pm 72$  pN respectively,  $p < 0.001$ ), indicating that the Cys152S mutation  
285 impacts the interaction strength. However, both WT and vWA-Cys152S PilY1 cells showed a  
286 similar binding probability to the hydrophobic AFM tip (**Fig. 2C**), a result that is consistent with  
287 both strains having similar levels of surface pili (**Fig. 1G**). Cells with the full deletion of the vWA  
288 domain ( $\Delta vWA_f$ ) showed an ~0% binding probability (**Fig. 2C**) to the hydrophobic tip and a low  
289 adhesion force (~45 pN, **Fig. 2B**), likely due to a low number of surface pili (**Fig. 1F**). These  
290 data suggest that the observed force curves are dependent on the TFP-associated PilY1.

291           For cells expressing the WT PilY1 and the vWA-Cys152S variant, which both showed  
292 adhesion to the hydrophobic AFM tip, two distinct adhesive behaviors were observed, plateaus  
293 (red arrow) and spikes (blue arrow; **Fig. 2D**). Plateaus are defined as adhesive events with a  
294 “step” behavior, that is, a constant sustained force over a defined length of time, while spikes  
295 are defined as sharp adhesive events with a single minimum and are reflective of a nanospring  
296 behavior [25]. Plateaus and spikes are not mutually exclusive in their appearance and

297 frequency. Cells expressing WT PilY1 or the vWA-Cys152S variant showed plateaus and  
 298 spikes, however, the frequency of these behaviors differed significantly between the strains  
 299 (**Fig. 2E**). Cells expressing the WT PilY1 had a similar proportion of plateaus (~61%) and spikes  
 300 (~52%; the sum can be >100% because some force curves can have both features). In contrast,  
 301 cells expressing the vWA-Cys152S mutant of PilY1 showed a significantly lower frequency of  
 302 plateaus (~15% compared to ~61% for the WT) and a much higher frequency of spikes (~93%  
 303 compared to ~52% for the WT; **Fig. 2E**). These data indicate that a single point mutation in the  
 304 PilY1 vWA domain can have a marked impact on the cell's mechanical behavior.

305 Finally, the magnitude of the adhesive signatures for both spikes and plateaus were higher  
 306 for cells with WT PilY1 than those cells expressing the vWA-Cys152S variant (**Fig. 2F and G**),  
 307 consistent with the observation that cells expressing WT PilY1 can sustain globally higher  
 308 adhesive forces than the cells expressing the vWA-Cys152S mutant (**Fig. 2B**). Interestingly, for  
 309 both strains the observed plateau forces are higher than those observed for the spikes, which,  
 310 along with the higher frequency of plateaus observed in WT PilY1, also explains the higher forces  
 311 sustained by the WT cells.

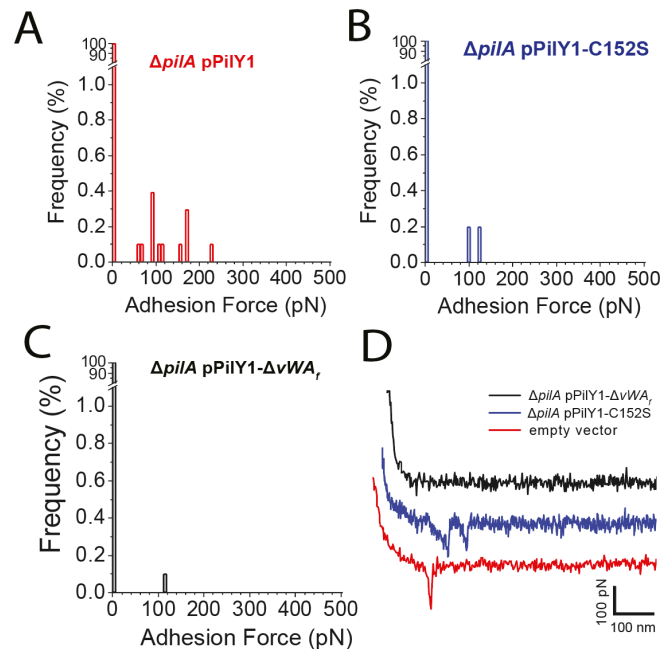


312 **Figure 2. Strains expressing the PilY1-Cys152S mutation display less adhesion force and altered mechanical**  
 313 **behaviors compared to strains expressing the WT PilY1.** **A.** Scheme of the AFM setup showing that pilated *P.*  
 314 *aeruginosa* is probed with a hydrophobic AFM tip at the free end of the AFM cantilever. Adhesive interactions  
 315 occurring between the pilus/cell body and the AFM tip cause a deflection of the cantilever, directly proportional to  
 316 force, which is recorded by a laser beam focused at the AFM tip's free end and reflected back to a photodiode. **B.**

317 Adhesion force histograms between the hydrophobic AFM tip and a representative WT strain, or strains expressing  
318 the Cys152S or  $\Delta vWA_f$  variants of PilY1. For WT:  $211 \pm 72$  pN ( $n = 55$  adhesive curves); for the vWA-Cys152S:  
319  $133 \pm 89$  pN ( $n = 47$ ) and for the  $\Delta vWA_f$ :  $45 \pm 89$  pN ( $n = 16$ ). **C.** Box plots comparing the binding probability of  
320 cells expressing the WT PilY1 or of strains expressing the Cys152S or  $\Delta vWA_f$  variants of PilY1 are shown. The  
321 number of probed cells is indicated. Stars are the mean values, lines the medians, boxes the 25-75 % quartiles and  
322 whiskers the standard deviation (SD). Student t-test: \*  $p \leq 0.05$ , \*\*  $p \leq 0.01$ . **D.** Representative retraction force  
323 profiles exhibited by the WT or Cys152S mutant cells sorted based on their shape. Plateaus are defined as adhesive  
324 events with a “step” behaviour, i.e., a constant sustained force over a defined length of time while spikes are defined  
325 as sharp adhesive events with a single minimum. A single retraction profile can feature several plateaus (red arrow),  
326 spikes (blue arrow) and even both signatures can occur as marked by the arrows. **E.** Box plots comparing the  
327 occurrence of plateaus (shaded) or spikes (striped) signatures for the WT and Cys152S mutant cells. The number of  
328 probed cells is as described in panel C. For the WT, plateaus =  $60.8 \pm 24.0$  % and spikes =  $51.9 \pm 16.6$  %,  $n = 11$ ,  
329 and for Cys152S, plateaus =  $14.9 \pm 13.3$  % and spikes =  $93.1 \pm 5.4$  %,  $n = 8$ . Stars are the mean values, lines the  
330 medians, boxes the 25-75% quartiles and whiskers the SD. Student t-test: \*\*  $p \leq 0.01$ , \*\*\*  $p \leq 0.001$ . **F** and **G.**  
331 Distribution of the adhesion forces exhibited by either the plateaus or the spikes for the WT (**F**) or the strain carrying  
332 the Cys152S mutant of PilY1 (**G**). The mean values are provided along with the histograms. All data were obtained  
333 by recording force-distance curves in medium containing M8 salts with an applied force of 250 pN and a pulling  
334 speed of  $5 \mu\text{m/s}$  at room temperature.  
335

336 Our data above indicate that the observed adhesive forces as well as the plateau and  
337 spike signatures observed for strains expressing WT PilY1 protein versus the vWA-Cys152S  
338 mutant protein were dependent PilY1 and its vWA domain. We next asked where these force  
339 profiles were dependent of the TFP. Because PilY1 is cell-surface-associated and can be  
340 secreted to the cell-surface independent of the TFP machinery [3], we expressed plasmid-borne  
341 WT PilY1 and the vWA-Cys152S mutant protein in a  $\Delta pilA$  background, lacking the full pilus  
342 fiber, and performed AFM experiments. Both strains expressing the WT PilY1 protein and the  
343 vWA-Cys152S mutant protein showed little adhesion to the hydrophobic tip (binding probability  
344  $< 1\%$ ; **Fig. S3A-C**). The scarce adhesive events recorded for the strains expressing these  
345 proteins in the  $\Delta pilA$  background were significantly lower than those exhibited when the pilus  
346 was present, and plateau signatures were never observed (**Fig. S3D**). Instead, typical receptor-  
347 ligand signatures were recorded, resembling a spike signature, but with very short rupture  
348 length consistent with the length of the protein that is stretched while the AFM tip retracts away  
349 from the bacterium (**Fig. S3D**). Together, the genetic and AFM data support the hypothesis that  
350 the adhesive forces measured, as well as the plateaus and spikes signatures exhibited by the

351 strains expressing the WT PilY1 protein and the vWA-Cys152S mutant protein, are due to both  
352 PilY1 plus the pilus fiber.  
353



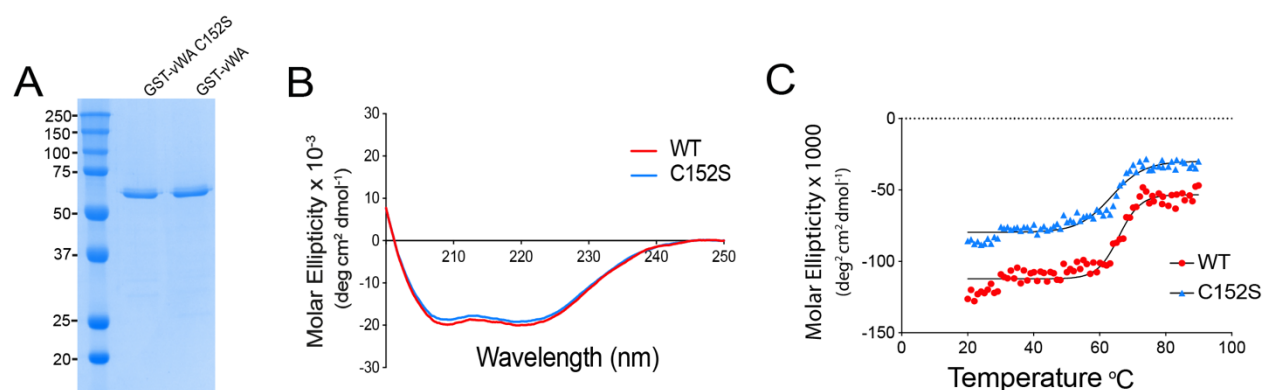
354

355 **Figure S3. The pilus fiber is required for adhesion to a surface.** A-C. Adhesion force histograms obtained by  
356 recording force-distance curves between the hydrophobic cantilever tip and representative  $\Delta pilA$ /pPilY1 (A),  
357  $\Delta pilA$ /pPilY1-Cys152S (B) and  $\Delta pilA$ /pPilY1- $\Delta vWA_r$  (C) cell. D. Representative retraction force profiles shown for  
358 the same strains.  
359

360 **The vWA-Cys152S mutation has a negligible impact on the solution conformation of the**  
361 **vWA domain.** Given our findings of the significant difference in mechanical behaviors observed  
362 for the strains expressing the WT PilY1 protein and the vWA-Cys152S mutant protein when these  
363 strains are engaged with a surface and thus under mechanical tension, we next determined  
364 whether this single cysteine mutation affected the conformation of purified, isolated vWA domain  
365 of PilY1 in solution. We focused on the vWA domain because despite attempts with several  
366 different expression systems, we were unable to purify stable, full-length PilY1 or the N-terminal  
367 domain of this protein. We cloned WT vWA and vWA-C152S domains (aa 30-369) as glutathione-  
368 S-transferase (GST) fusion proteins to enhance stability and facilitate purification. A GST domain  
369 and a HRV-3C protease cleavage site were added to the N-terminus of vWA and the resulting

370 fusion proteins were overexpressed in *E. coli* cells and purified to homogeneity (**Fig. 3A**). The  
371 HRV-3C protease cleavage site was confirmed by sequencing. Unfortunately, repeated attempts  
372 to efficiently cleave the GST domain from the vWA proteins with protease HRV 3C were  
373 unsuccessful, perhaps due to steric occlusion of the protease binding site in the purified proteins.  
374 Thus, the studies below were done using GST-vWA fusion proteins.

375 We performed far-UV circular dichroism (CD) spectroscopy to determine the secondary  
376 structure of the WT and mutant fusion proteins and to assess the thermal stability of WT-vWA  
377 and the vWA-Cys152S variants (**Fig. 3B** and **3C**). Far-UV CD spectra of the GST-WT-vWA and  
378 GST-vWA-Cys152S fusion proteins were monitored at wavelength scans between 195 and 250  
379 nm. Both WT and mutant spectra showed the presence of two distinct negative peaks centered  
380 at 208 and 222 nm, typical of  $\alpha$ -helical proteins (**Fig. 3B**). Overall, the dichroic spectra for GST-  
381 WT-vWA and GST-vWA-Cys152S were similar. Measuring CD as a function of temperature can  
382 be used to determine the effects of mutations on protein stability. Analysis of the ellipticity curves  
383 in the range of 20 to 90 °C showed the melting temperatures of GST-WT-vWA and GST-vWA-  
384 C152S fusion variant to be similar (65.8 versus 63.5 °C; **Fig. 3C**), suggesting that the C152S  
385 mutation did not perturb the secondary structure of the domain in solution (i.e., in the absence of  
386 mechanical force).



387 **Figure 3. vWA-C152S mutation does not substantially alter conformation of the vWA domain.** A. Coomassie  
388 Blue-stained SDS-PAGE of ~ 1  $\mu$ g of purified wild-type GST-vWA and GST-vWA-C152S fusion proteins  
389 expressed from a pGEX plasmid backbone and purified from *E. coli* BL21-DE3 cells as detailed in the Materials and

390 Methods. The molecular weight markers are indicated. **B.** Far-UV Circular dichroism (CD) spectra shown in molar  
391 ellipticity for the WT GST-vWA (red line) and GST-vWA-C152S mutant (blue line) between 195 and 250 nm at 20  
392 °C. **C.** Curves of ellipticity at 208 nm wavelength as a function of temperature for WT and mutant fusion proteins.  
393 Spectra were recorded for each sample from 20 to 90 °C in 1 ° increments. Curves were fitted to a Boltzmann  
394 sigmoidal equation and the  $V_{50}$  value was determined (65.8 versus 63.5 °C for GST-WT-vWA and GST-vWA-  
395 C152S fusion variant, respectively).  
396

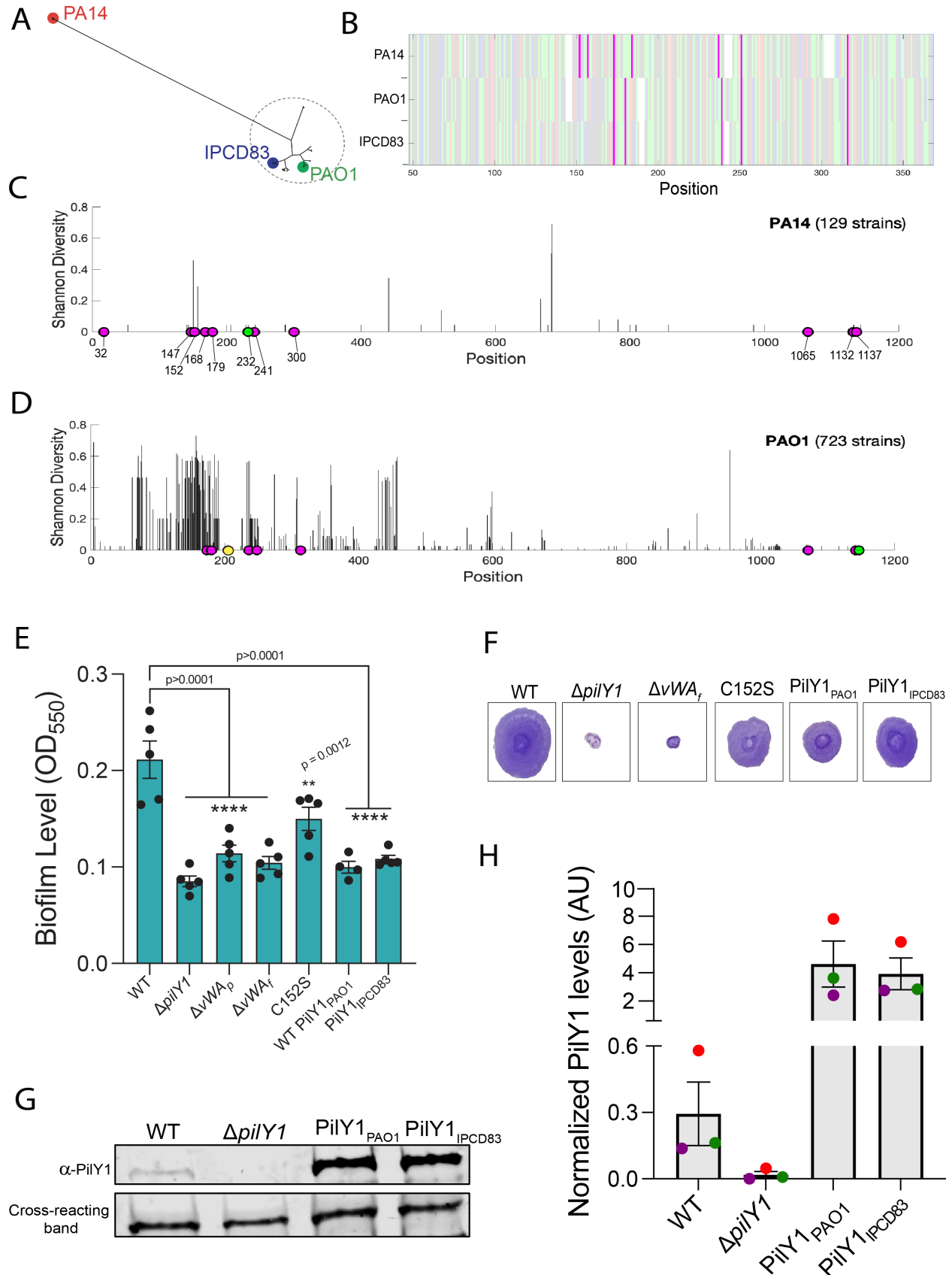
397 **Genomic analyses reveal that PAO1 strains lack the vWA-C147 and vWA-Cys152 cysteine**  
398 **residues that are present in PA14 strains, with associated functional consequences.**

399 Given our findings that cells expressing the vWA-Cys152S mutation impact surface sensing, c-  
400 di-GMP levels and biofilm formation (**Fig. 1B-C, Fig. S1B**) in *P. aeruginosa* PA14, we analyzed  
401 whether the Cys152 residue was conserved across *P. aeruginosa* strains. We leveraged PilY1  
402 sequences from the international *P. aeruginosa* consortium database (IPCD), a repository for  
403 thousands of *P. aeruginosa* isolates from a diverse range of environments [26]. We analyzed  
404 the phylogenetic relationship of PilY1 amino acid sequences from a total of 852 *P. aeruginosa*  
405 genomes and found two distinct clades, PA14 (red dot) and PAO1 (dashed circle; **Fig. 4A**),  
406 largely consistent with a previous report by Levesque and colleagues [26]. The PilY1 sequence  
407 from the strain, IPCD83 (blue dot), falls within the PAO1 clade. Alignment of the amino acid  
408 sequences of the vWA domain of PilY1 from the PA14, PAO1 and the IPCD83 strains show that  
409 five of the seven cysteines (magenta) in the vWA domain of PA14 are highly conserved in  
410 PAO1 and IPCD83, although the spacing of the residues varies in some cases (**Fig. 4B**). All  
411 three domains consist of positive, negative, polar and hydrophobic amino acids shown in red,  
412 blue, green and grey, respectively. Of note is the high abundance of polar residues in the vWA  
413 domains of all three strains.

414 To examine the amino acid diversity of the PilY1 sequences in the PA14 and PAO1  
415 clades, we computed Shannon diversity index as a measure of sequence diversity (**Fig. 4C** and  
416 **4D**). We aligned PilY1 sequences within the PA14 (**Fig. 4C**) and PAO1 (**Fig. 4D**) clades and  
417 calculated Shannon diversity at each amino acid position.

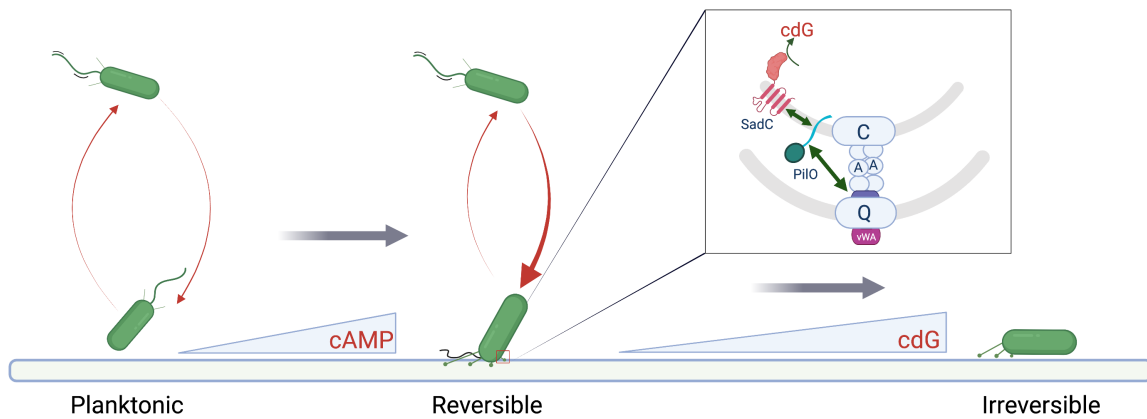


418           As shown in Figure 4C, there is very little amino acid sequence diversity over the entire  
419 PilY1 sequence among the 129 isolates with PA14 versions of PilY1. Interestingly, all strains in  
420 the PA14 clade except one contain the 11 cysteines (magenta circles) found in the PA14  
421 reference strain (**Fig. 4C**). Furthermore, each isolate had all seven cysteines in the vWA domain  
422 while there was one strain missing vWA-C232 residue (green circle; a residue we found critical  
423 for TFP-mediated twitching motility, **Fig. S1B**). In contrast to the PA14 clade, strains within the  
424 PAO1 clade showed low diversity at the C-terminal domain (amino acid 626-997) and high  
425 amino acid diversity in the vWA domain (amino acid 48-368; **Fig. 4D**). Additionally, of the 723  
426 variants of the PilY1 sequences from the PAO1 clade analyzed, only eight cysteines were highly  
427 conserved compared to the 11 highly conserved cysteines for the PA14 strains. The vWA  
428 domain of the PAO1 clade contains five of the seven conserved cysteines found in the PA14  
429 clade. Interestingly, vWA-147 and vWA-Cys152 residues are not present in any of the PAO1  
430 strains, including the IPCD83 isolate. Recall, that we showed that both vWA-C147 and vWA-  
431 Cys152 residues are important in c-di-GMP signaling, and mutations in these residues resulted  
432 in strains with decreased biofilm formation but retaining twitching motility (**Fig. 1B** and **Fig.**  
433 **S1B**).



435 **Figure 4. Comparative genomic analyses reveal sequence and functional differences between PA14 and PAO1**  
436 **alleles of PilY1.** **A.** Phylogenetic tree of PilY1 amino acid sequences obtained from the IPCD database of *P.*  
437 *aeruginosa* genomes [26] showing two distinct clades of PilY1 sequences corresponding to strains from the previously  
438 determined *P. aeruginosa* PA14 and PAO1 clades. The strain labeled IPCD83 is an isolate within the PAO1 clade. **B.**  
439 Alignment of the vWA domain (48 to 368) of PilY1 proteins found in PA14, PAO1 and IPCD83 strains, with cysteines  
440 highlighted in magenta. Positive, negative, polar and hydrophobic amino acids are depicted in red, blue, green and  
441 grey, respectively. **C.** Shannon diversity index along the PilY1 amino acid sequence for the 129 PilY1 proteins  
442 belonging to the PA14 clade. Fully conserved cysteines are highlighted in magenta. One strain is missing the cysteine  
443 depicted in green. **D.** Shannon diversity index along the PilY1 amino acid sequence for the 723 versions of PilY1  
444 proteins belonging to the PAO1 clade. Fully conserved cysteines are highlighted in magenta. One strain is missing the  
445 cysteine depicted in green, and one strain has an extra cysteine depicted in yellow. **E.** Biofilm formation measured at  
446 OD<sub>550</sub> in a static 96 well assay for the indicated strains. Hybrid *P. aeruginosa* PA14 strains carry the PilY1 protein  
447 from PAO1 (PilY1<sub>PAO1</sub>) or the PilY1 protein from IPCD83 strain (PilY1<sub>IPCD83</sub>) replacing the coding region for the *P.*  
448 *aeruginosa* PA14 PilY1 protein. In all cases, the mutant PilY1 variants are expressed from the native locus of *P.*  
449 *aeruginosa* PA14. Error bars are SEM and statistical significance shown was determined by one-way ANOVA and a  
450 Dunnett's post-hoc test. p values: p ≤ \*\*\*\* 0.0001, p ≤ \*\*\* 0.001, p ≤ \*\* 0.01, ns, not significant. **F.** Representative  
451 images of twitch zones shown for the indicated strains. **G.** Representative Western blot image for steady state PilY1  
452 protein levels in whole cells WT PilY1,  $\Delta pilY1$ , PilY1 from PAO1 (PilY1<sub>PAO1</sub>) and PilY1 variant from strain IPCD83  
453 (PilY1<sub>IPCD83</sub>). **H.** Quantification of normalized PilY1 protein levels from whole cells for strains shown in G. Protein  
454 level is normalized to a cross-reacting band at ~60 kDa. Data are from three biological replicates in three independent  
455 experiments. Dots with the same color represent the same biological replicate; different colors indicate different  
456 biological replicates.  
457

458           Given the biofilm phenotype of the strain expressing the vWA-Cys152 variant of PilY1  
459 (**Fig. 1B** and **Fig. S1B**) and the role of PilY1 in early biofilm formation and c-di-GMP signaling,  
460 we expected that loss of the vWA-Cys152 residue in strains from the PAO1 clade, including  
461 IPCD83, should result in similar phenotypes. To test this hypothesis, we cloned the *pilY1* gene  
462 from the IPCD83 isolate (PilY1<sub>IPCD83</sub>) or the WT PAO1 strain (WT PilY1<sub>PAO1</sub>) into the native locus  
463 of the reference PA14 strain and performed static biofilm assays. Like the vWA-Cys152S  
464 mutation, both PAO1 variants expressed in the PA14 strain resulted in significantly decreased  
465 levels of biofilm formation as compared to WT (**Fig. 4E**). Quantification of c-di-GMP levels for  
466 PilY1<sub>IPCD83</sub> showed a significant decrease in c-di-GMP level (**Fig. 1C**). Additionally, both the  
467 PilY1<sub>PAO1</sub> and PilY1<sub>IPCD83</sub> variants still supported twitching motility at a level that is similar to the  
468 vWA-Cys152S mutant protein (**Fig. 4F**). The PilY1<sub>PAO1</sub> and PilY1<sub>IPCD83</sub> variants showed levels of  
469 PilY1 expression that exceed the WT (**Fig. 4G** and **Fig. 4H**), indicating that the observed  
470 phenotypes were not due low-level expression of these variants.  
471



472  
473 **Figure 5. Proposed model for force-induced mechanical force drive transition from planktonic to**  
474 **irreversible attachment.** Planktonic bacteria interact with the surface and increase cAMP levels and  
475 surface pili levels. The proposed PilY1-PilO interaction can in turn drive the documented PilO-SadC  
476 signal transduction cascade which stimulates c-di-GMP signaling and increased biofilm formation.  
477

478

## 479 Discussion

480  
481

Our data show that force-induced changes mediated by one or more cysteine residues  
482 in the vWA domain of the TFP tip-associated protein, PilY1, are required for surface sensing  
483 and downstream c-di-GMP signaling and biofilm formation. The concept of mechanical force  
484 inducing protein conformational changes, that these changes are modulated by disulfide bonds  
485 and that such changes in conformation are required for function is well studied in the eukaryotic  
486 proteins, titin and vWF. Titin undergoes cycles of folding and refolding that allows it to function  
487 as a molecular spring during cycles of muscle relaxation and contraction, respectively [27, 28].  
488 When force is applied, the immunoglobulin (Ig) domains of titin unfold and extend [29]. Similarly,  
489 increased shear forces due to blood flow cause the vWF to transition from a globular to a  
490 stretched conformation [30]; this stretched conformation allows the vWF to bind to platelets and  
491 form a clot at sites of vascular damage [31]. Furthermore, the folding and refolding events  
492 observed for titin and vWF are mediated by disulfide bonds [32, 33]. For titin, oxidation of the  
493 disulfide bond greatly increases both its speed and magnitude of folding [34] while the redox  
494 state of the disulfide bond in the A2 domain of the vWF determines exposure of platelet binding

495 sites [21]. Additionally, disulfides bonds in FimH, the adhesin on the type-I pilus in *E. coli* [35],  
496 are essential for adhesion under high flow environments [36].

497         The vWA domain of PilY1 in *P. aeruginosa* PA14 has seven cysteine residues. Our  
498 genetic analyses show that two of these residues, vWA-Cys152 and to a lesser extent vWA-  
499 Cys147, are critical for PilY1-dependent surface signaling and biofilm formation. Our AFM  
500 studies support the conclusion that strains expressing the vWA-Cys152S mutant results in cells  
501 that are still capable of surface attachment at the same frequency as the WT, and furthermore,  
502 this mutation does not destabilize the PilY1 protein. Using AFM, we show that the WT cells  
503 display spike signatures, which are typical of nanospring behaviors [25]. That is, T4P/PilY1 can  
504 display elastic properties upon the application of force, but once the force is removed, the pilus  
505 rapidly returns to its original conformation. Based on previous work [25] and our data here,  
506 these force profiles appear to require both TFP and PilY1. Such nanospring properties are also  
507 observed for SpaC, a vWA domain-containing protein that is a key pilus-associated adhesin of  
508 *Lactobacillus rhamnosis* GG [23]. Under high mechanical forces, SpaC is shown to behave like  
509 a spring. This spring-like behavior is thought to allow the bacterium to withstand higher forces  
510 under shear stress when the pilus is stretched, and presumably allow the pilus to engage the  
511 surface under strain without snapping [23].

512         The WT *P. aeruginosa* PA14 strain also shows plateau signatures. One interpretation of  
513 these plateau signatures is that they reflect the pilus being bound to the surface at multiple  
514 points followed by successive desorption of the pilus [37]. Alternatively, plateaus signatures may  
515 be indicative of sustained protein conformational changes. In either case the plateaus observed  
516 for WT cells produce high adhesive force signatures, thus likely helping to promote surface  
517 engagement.

518         We found that mutating the Cys152 residue of the vWA domain of PilY results in a  
519 reduction in biofilm formation and lower levels of c-di-GMP production. A strain expressing this  
520 mutant variant also shows significant changes in mechanical properties (detailed below) when

521 the cell is subjected to force. That these changes in mechanical behavior are dependent on  
522 applying a force is in line with our CD and melting curve data which, show no differences in the  
523 overall global and secondary structures for WT and the Cys152Ser variant when in solution (i.e.,  
524 in the absence of an applied force).

525 The findings from our AFM analysis of the WT and vWA-Cys152Ser allele of PilY1 raise  
526 some interesting implications. The ~50-50% distribution of plateaus and spikes observed in  
527 cells with WT PilY1 could suggest a built-in property that allows for inherent heterogeneity in  
528 surface adaptation. That is, transient changes in PilY1 conformation (the spike signatures) may  
529 not be sufficient to drive signaling; only sustained conformational changes (i.e., plateaus) can do  
530 so. Our observation that the vWA-Cys152S mutant variant of PilY1 is skewed ~90:10 towards  
531 spike signatures (i.e., transient conformational changes), and that this strain is defective for c-di-  
532 GMP signalling, supports this conclusion. Thus, not every interaction between a cell and the  
533 surface to which it might attach is “productive”, a conclusion consistent with several reports  
534 showing the heterogenous nature of *P. aeruginosa* populations transitioning to a biofilm lifestyle  
535 [20, 38-40]. Furthermore, we could predict then that a PilY1 mutant that favors the plateau  
536 conformation should promote c-di-GMP signaling and be a hyper-biofilm former. We have  
537 performed extensive genetic screens looking for PilY1 mutants with such phenotypes with no  
538 success to-date. Thus, an alternative explanation is that the ability of TFP/PilY1 to transition  
539 *between* conformations is key to the ability to signal properly, and that locking the protein in one  
540 conformation, or another, results in aberrant signaling.

541 The critical role for vWA-Cys152 in c-di-GMP signaling and biofilm formation is  
542 supported by our genomic analysis, which highlight differences in the PilY1 protein among PA14  
543 and PAO1 strains. The vWA domain of PilY1 from the PA14 and PAO1 strains are very  
544 different, with PilY1 proteins from the PAO1 clade (PAO1 and IPCD83) lacking the conserved  
545 vWA-Cys152 and vWA-Cys147 residues. *P. aeruginosa* PA14 strains engineered to carry the  
546 PAO1 or IPCD83 alleles of PilY1, which lack the conserved vWA-Cys152 and vWA-Cys147

547 residues, result in a hybrid strain that behaves very much like the *P. aeruginosa* PA14 strain  
548 carrying the vWA-Cys152S mutant protein. Thus, our genetic analysis confirmed that the  
549 observed sequence differences have functional consequences. The distinct PilY1 proteins of *P.*  
550 *aeruginosa* PA14 and PAO1 may also contribute to explaining the differences in the surface  
551 commitment strategies observed for these strains, as reported previously [3, 39].

552 Our AFM data show that force curve plateaus can be maintained for up to 50 ms; it is  
553 important to note that this value may be an underestimation because desorption of the pilus  
554 from the AFM tip may result in the force curve returning to baseline. With this important caveat  
555 in mind and considering that the *P. aeruginosa* TFP has a known retraction rate of  $\sim 0.5 \mu\text{m}$   
556  $\text{s}^{-1}$  [41], then the distance that the TFP is retracted during this 50 ms window (the time spane  
557 plateaus are maintained) is  $\sim 0.025 \mu\text{m}$ . This is quite a short distance (TFP can exceed two  
558 microns) and corresponds to the pilus being (almost) fully retracted, with the priming complex  
559 (i.e., the minor pilins) and the vWA domain of PilY1 docked into the pore of the secretin [5].  
560 Furthermore, if we postulate that TFP/PilY1-mediated signaling is a consequence of mechanical  
561 force, for the TFP/PilY1 to remain under force and thus potentially capable of propagating a  
562 signaling event via a conformational change, we hypothesize that at least one other pilus would  
563 need to be bound to the surface to pull in opposition to the fully retracted pilus described above.  
564 That is, PilY1-mediated signaling would require multiple pili to decorate the cell surface – this  
565 model has a key corollary in that TFP must be robustly expressed for signaling to occur.  
566 Interestingly, previous studies [42-45] and work from our team [3] shows that the level of TFP is  
567 low in planktonic cells. Furthermore, our team showed that increased cAMP levels via the Pil-  
568 Chp system [3], which is key for pilus production, might require several cellular generations and  
569 multiple transient surface interactions to occur [39]. Thus, our previous observations of a role of  
570 multigeneration cAMP signaling via TFP may be *necessary* to produce multiple TFP; multiple  
571 TFP, in turn, are *required* for subsequent c-di-GMP signaling.



572           Based on the data presented here and previous studies from our team and others [3, 20,  
573 39], we propose the following model of the early events initiating biofilm formation by *P.*  
574 *aeruginosa* PA14 (**Fig. 5**). When the TFP of *P. aeruginosa* PA14 initially engage the surface,  
575 we propose that the Pil-Chp signaling cascade promotes cAMP production, which in turn  
576 enhances transcription and subsequent production of TFP over the low levels of these  
577 appendages produced by planktonically-grown bacteria [3]. Currently, we do not have a strong  
578 mechanistic understanding of the linkage(s) among TFP, the Pil-Chp system and cAMP  
579 production. However, once more pili are deployed to the surface, this event provides the  
580 necessary condition for multiple surface-engaged TFP working in opposition to generate  
581 mechanical tension. This mechanical tension in turn can drive the sustained, PilY1-Cys152-  
582 dependent conformational changes we have observed for WT cells. That is, the conformational  
583 change in vWA domain of PilY1 is maintained only during the application of force when the  
584 TFP pull against a solid surface and thereby generate tension (with the cells presumably not  
585 moving). We propose that when multiple TFP are engaging the surface, the change in  
586 TFP/PilY1 conformation can be sustained as the pilus retracts and PilY1 is docked in the PilQ  
587 pore; here PilY1 can interact with PilO, as has been reported for the homologous system in  
588 *Myxococcus xanthus* [5]. Based on our recent study [20], the proposed PilY1-PilO interaction  
589 can in turn drive the documented PilO-SadC signal transduction cascade [20], which stimulates  
590 c-di-GMP signaling and increased biofilm formation. It is also important to note that a recent  
591 pull-down analysis indicate that there is one molecule of PilY1 per pilus in *M. xanthus* [5], thus it  
592 is unlikely that intermolecular disulfides are being formed with other PilY1 proteins. Additionally,  
593 cryo-electron tomography shows the C-terminal domain of PilY1 to be in direct contact with the  
594 minor pilins while the vWA domain is at the apex of the pilus fiber [5], suggesting that  
595 intermolecular disulfide bond formation between PilY1 and any of the minor pilins is also  
596 unlikely. Consistent with this conclusion, our purification of the vWA domain and Western  
597 analysis of cell-surface PilY1 shows no evidence of PilY1 forming intermolecular multimers.

598 Finally, our studies were able to successfully separate the role of TFP in motility from its  
599 role in signaling. Work from our team and others [2, 3, 18, 20, 46] have implicated TFP in  
600 surface sensing via the surface-dependent stimulation of the second messengers cAMP and c-  
601 di-GMP, however, in these studies the mutants used also disrupted TFP-mediated twitching  
602 motility. Here, the Cys152S allele of PilY1 results in a clear loss of c-di-GMP signaling but  
603 strains carrying this mutation display robust twitching motility. Together with our previous  
604 studies showing a role of the TFP alignment complex component PilO in c-di-GMP production  
605 [20], we believe it is quite clear that TFP are not only a key appendage for adhesion and surface  
606 motility, but also a central player in surface-specific signal transduction.

607

## 608 **Materials and Methods**

609 **Bacterial strains, plasmids, media and growth conditions.** All bacterial strains used in this  
610 study are listed in the supplementary material in Table S1. *P. aeruginosa* PA14, *E. coli* S17- $\lambda$ -pir  
611 were routinely grown in 5 mL lysogeny broth (LB) medium or struck on 1.5% LB agar plates with  
612 appropriate antibiotics, if necessary. Overnight cultures were grown in LB at 220 rpm on a roller  
613 drum. *Saccharomyces cerevisiae* InvSc1 (Thermo Fisher) used for cloning was maintained on  
614 yeast peptone dextrose (YPD - 1% Bacto yeast extract, 2% Bacto peptone, and 2% dextrose)  
615 with 2% agar. Synthetic defined medium without uracil (Sunrise Science Products) was used to  
616 select for yeast with construct. All chromosomal point mutation were constructed using the  
617 pMQ30 shuttle vector while pMQ72 multi-copy plasmid was used for ectopic expression. All  
618 plasmids and oligonucleotides used in this study are listed in Table S2 and Table S3  
619 respectively.

620

621 **Construction of deletion mutant strains.** All chromosomal in-frame gene deletions were  
622 constructed using the pMQ30 shuttle vector carrying the flanking regions of the gene via  
623 homologous recombination using the yeast machinery [47] or by Gibson cloning as previously

624 described in [48] . For yeast cloning, *S. cerevisiae* was grown overnight at 30 °C in YPD.  
625 Synthetic defined medium without uracil (Sunrise Science Products) was used to select for  
626 yeast colonies with the plasmid construct. Plasmids were extracted from yeast using the ‘smash  
627 and grab’ method and transformed by electroporation into *E. coli* S17 cells and grown on LB  
628 plates with 10 µg/ml gentamycin at 30 °C overnight [2]. Colony polymerase chain reaction  
629 (PCR) amplification and sequencing was used to confirm plasmid construction. Plasmids were  
630 introduced in *P. aeruginosa* by conjugation and merodiploids were selected on 25 µg/ml  
631 gentamycin and 20 µg/ml nalidixic acid after which cells were counter-selected on LB with 10%  
632 sucrose-containing medium with no added salt [3]. Deletions were confirmed by colony PCR  
633 amplification and sequencing with primers flanking the gene. All sequencing was done at the  
634 Molecular Biology Core at the Geisel School of Medicine at Dartmouth.

635  
636 **Construction of chromosomal point mutations.** Point mutations in the *pilY1* gene were made  
637 using a modified *in vitro* site-directed mutagenesis protocol [49]. Forward and reverse  
638 complementary primers consisting of the nucleotide codon sequence encoding for the mutation  
639 of interest were used to separately amplify the pMQ30 (for chromosomal mutations) or pMQ72  
640 (ectopic expression) parental plasmids with the gene of interest using high fidelity Phusion  
641 polymerase (NEB). After four cycles of amplification, the products of these reactions were  
642 combined and amplified for an additional 18 cycles with additional Phusion polymerase added.  
643 The parental plasmid was digested for 4 h using Dpn1 endonuclease (NEB) at 37 °C. Following  
644 digestion, the PCR product was transformed into *E. coli* S17 competent cells and selected on  
645 LB with 10 µg/ml gentamycin. Plasmid containing the desired point mutation was isolated and  
646 confirmed by sequencing. Introduction of mutations on the chromosome was done by  
647 conjugation and counter-selection as described above. All chromosomal mutations were verified  
648 by PCR amplification and sequencing.

649

650 **Biofilm assay.** Overnight cultures (1.5 µl) were inoculated in U-bottom 96 well plates (Costar)  
651 containing 100 µl M8 salts minimal medium (Na<sub>2</sub>HPO<sub>4</sub>, KH<sub>2</sub>PO<sub>4</sub> NaCl) supplemented with  
652 glucose (0.2% v/v), casamino acids (0.5% v/v) and MgSO<sub>4</sub> (1 mM), subsequently referred to as  
653 M8 medium. Biofilm assay plates were then stained with 100 µl of 0.1% crystal violet in water  
654 for 20 mins at room temperature and destained for 20 mins with 125 µl de-staining solution  
655 (40% glacial acetic, 40% methanol and 20% H<sub>2</sub>O v/v). Absorbance was read at OD<sub>550</sub> and  
656 destaining solution was included as the blank. Biofilm assays were done similar to published  
657 work by the O'Toole group [50, 51].

658

659 **In vivo c-di-GMP quantification.** Nucleotides were extracted from *P. aeruginosa* cells scraped  
660 from 0.52% agar with M8 medium after incubation for 37°C for 14 h. Cells were removed from  
661 plates by gently scraping with a cover slip to avoid scraping the agar, and then immediately  
662 placed on ice. Cell pellets were re-suspended in 250 µl nucleotide extraction buffer  
663 (methanol/acetonitrile/dH<sub>2</sub>O 40:40:20 + 0.1 N formic acid) and incubated at -20°C for 1 h.  
664 Following nucleotide extraction, cells were spun for 5 mins at 4°C, 200 µl of supernatant was  
665 removed and then added to 8 µl of 15% NH<sub>4</sub>HCO<sub>3</sub> stop solution. Nucleotides were dried in a  
666 speed vacuum and resuspended in 200 µl HPLC grade water (JT Baker) and placed in screw  
667 cap vials (Agilent Technologies). Quantification of c-di-GMP levels was done by liquid  
668 chromatography-mass spectrometry (LC-MS/MS) by Lijun Chen at the Mass Spectrometry  
669 Facility at Michigan State University. All samples were normalized to dry weight and expressed  
670 as  $\frac{pmol}{mg\ dry\ weight}$ .

671

672 **Macroscopic twitch assay.** One percent LB agar plates were stab inoculated using toothpicks  
673 dipped in overnight cultures to the bottom of the plate. Plates were incubated at 37°C for 24 h  
674 and an additional day at room temperature. The agar was subsequently removed from the petri

675 plate and the twitch zones stained with crystal violet to visualize, and the diameter of the twitch  
676 zones measured.

677  
678 **Plaquing assay.** One percent agar plates (60 x15 mm) with M8 medium were prepared and  
679 cooled to room temperature. Fifty microliters of *P. aeruginosa* overnight culture were added to 1  
680 mL of 0.5% warm top agar made with M8 medium and gently mixed. The mixture was quickly  
681 poured onto 1% agar plates made with M8 salts. Plates were swirled to ensure even spreading  
682 of top agar. Once cooled, 2  $\mu$ l of phage DMS3<sub>vir</sub> strain were spotted to the center of the plate,  
683 allowed to dry and subsequently incubated at 37 °C overnight.

684  
685 **Cell surface pili.** WT,  $\Delta$ *pilY1*, *vWA* variants and *vWA*-Cys152S cells were streaked in a grid-  
686 like pattern on 10% agar plates with M8 SALTS/supplements and incubated at 37 °C overnight.  
687 Four plates per strain were struck for each biological replicate to ensure adequate number of pili  
688 could be recovered. The following day cells were scraped off the plate using a cover slip and put  
689 in a 2 mL tube and vortexed vigorously for 2 mins with 1 mL of phosphate buffer saline (PBS –  
690 Corning). Cells suspensions were subsequently spun at 16, 000 x g for 5 mins in a table-top  
691 centrifuge and the supernatant removed and transferred to a clean tube and spun again. This  
692 step was repeated until no pelleted cells were recovered. Proteins were precipitated with 20%  
693 trichloroacetic acid (TCA – VWR) on ice overnight at 4° C. Precipitated proteins were collected  
694 by centrifuging at 16 000 x g for 25 mins at 4° C. The supernatant was discarded and the tubes  
695 re-centrifuged for 3 mins to get rid of any remaining supernatant. Pellets were washed twice  
696 with 1 mL acetone (VWR) and subsequently air dried to remove residual acetone. Pellets were  
697 resuspended in 100 ml 1x sample buffer (BioRad) with b-mercaptoethanol and boiled for 5 mins  
698 and then briefly spun before being ran on a 12% SDS-PAGE gel, and the samples probed for  
699 PilA and FliC by Western blot analysis. FliC served as the loading control and was used for  
700 normalization of PilA protein levels. Samples were also resolved on a 7.5% SDS-PAGE gel and

701 probed for PilY1 using a-PilY1 antibody generously provided by Matt Wolfgang. Western blot  
702 analysis was performed as described below.

703

704 **Western Blot analysis for PilY1 protein levels in whole cell lysate.** All strains were grown

705 overnight in LB at 37 °C. For whole cell lysate (WCL) preps, overnight cultures were diluted

706 1:100 in 5 mL M8 SALTS/supplements minimal medium and sub-cultured for ~3 h at 37 °C.

707 Samples were resolved on a 7.5% Tris-HCl precast SDS-PAGE gel (Bio-Rad) and blotted onto

708 0.45 µm pore size nitrocellulose membrane (Bio-Rad) using the 1.5 mm pre-programmed

709 method on a Trans-Blot Turbo Transfer System (Bio-Rad). The membrane was incubated in

710 blocking buffer (LI-COR Blocking Buffer in TBS) for 1 h at room temperature and incubated for 1

711 h or overnight at 4 °C in polyclonal a-PilY1 antibody (1:5000 dilution) in BSA TBST<sub>0.1%</sub> buffer.

712 Following incubation with primary antibody, the membrane was washed in TBST<sub>0.1%</sub> for 5 mins

713 x3 and incubated for 1 h with goat anti-rabbit in TBST<sub>0.1%</sub> (1:10,000 dilution) secondary antibody

714 (LI-COR IRDye® 800CW Goat a-rabbit). Incubation with secondary antibody and all subsequent

715 steps were performed in the dark. After incubation with the secondary antibody, the membrane

716 was washed in TBST<sub>0.1%</sub> for 5 mins x2 and then once in TBS. The membrane was imaged using

717 the LI-COR Odyssey CLx imager at BioMT Core at the Geisel School of Medicine at Dartmouth.

718 PilY1 protein levels were quantified relative to the cross-reacting band at ~60 kD using the LI-

719 COR Image Studio Lite software by drawing a rectangle of the same size around each band and

720 using the following background settings: average, border width of 3, segment = all.

721

722 **Protein quantification.** Total protein levels in whole cell lysate was quantified using the Bio-

723 Rad protein assay Dye Reagent as per the manufacturer's instructions as outlined by Bradford

724 [52].

725

726 **AFM force spectroscopy (AFM).** Overnight cultures used in AFM experiments were diluted 200-

727 fold in M8 salts and seeded on hydrophobic non-treated polystyrene petri dishes (Corning) and

728 left for 10 minutes to adhere [25]. Dishes were then washed gently but thoroughly with M8 salts  
729 medium to remove most non-adhered bacteria and used for AFM experiments in the same  
730 medium. AFM experiments were performed at room temperature using a NanoWizard® 4  
731 NanoScience AFM (JPK Instruments). Gold cantilevers (PNP-TR probes – Pyrex Nitride Probe  
732 with Triangular Cantilevers – from NanoWorld) were treated for 16 h with a 1 mM 1-dodecanethiol  
733 solution in ethanol to render them hydrophobic, then rinsed with ethanol and kept in milliQ water  
734 until AFM experiments were ready to be performed. Prior any measurements, the cantilever's  
735 spring constant was empirically determined by the thermal noise method [53]. The AFM force  
736 volume mode was used to record force-distance curve in a pixel-by-pixel manner (force mapping)  
737 on  $6 \times 6 \mu\text{m}^2$  areas ( $32 \times 32$  pixels, i.e. 1024 curves) with a bacterium at the center, previously  
738 localized by an optical microscope coupled to the AFM. For the  $\Delta pilA$  strains overexpressing WT  
739 PilY1 or PilY1-Cys152S and lacking the pilus fiber, the area was decreased to  $1 \mu\text{m}^2$  around the  
740 bacterium's poles. The following settings were used: an applied force of 250 pN, a constant  
741 approach/retract speed of  $5 \mu\text{m/s}$  and a z-range of  $1.5 \mu\text{m}$ .

742

743 **AFM data analysis.** Data were analyzed with the data processing software from JPK  
744 Instruments (Berlin, Germany). In a first approach, all force distance curves exhibiting an  
745 adhesive event were selected, as opposed to the non-adhesive curves which were discarded,  
746 thus allowing an estimation of the binding probability. In a second approach, adhesive curves  
747 were sorted depending on their signature (plateaus vs spikes) and the maximum adhesion  
748 sustained by each adhesive peak was determined. The frequency of plateaus was assessed by  
749 dividing the number of curves showing plateaus plus curves showing both plateaus and spikes  
750 by the total number of adhesive curves. A similar approach was used to calculate the percent of  
751 spikes. The formulas to calculate the percent plateaus ( $P_{\text{plateaus}}$ ) or the percent spikes ( $P_{\text{spikes}}$ )  
752 are shown below:



753 (1)  $P_{\text{plateaus}} = (N_{\text{curves showing only plateaus}} + N_{\text{curves showing plateaus and spikes}}) / (N_{\text{curves showing only plateaus}} +$   
754  $N_{\text{curves showing plateaus and spikes}} + N_{\text{curves showing only spikes}})$

755 (2)  $P_{\text{spikes}} = (N_{\text{curves showing only spikes}} + N_{\text{curves showing plateaus and spikes}}) / (N_{\text{curves showing only plateaus}} + N_{\text{curves}}$   
756  $\text{showing plateaus and spikes}} + N_{\text{curves showing only spikes}})$

757 Statistical analyses were performed with Origin.

758

759 **Analysis of IPCD database: generation of phylogenetic tree, alignment and calculation of**

760 **Shannon Diversity.** We performed nucleotide BLAST searches on a local version of the IPCD

761 database of *P. aeruginosa* genomes to identify variants of the PilY1 protein. Using the

762 nucleotide sequences of PilY1 from PA14, PAO1 and IPCD-83 (GenBank: MCMY00000000),

763 we were able to identify 852 strains with versions of the full protein. We used custom MATLAB

764 scripts to perform an alignment of the amino acid sequences of all 852 versions of PilY1 and

765 construct the corresponding phylogenetic tree. We performed the alignment of PilY1 amino acid

766 sequences using a series of BLOSUM80 to BLOSUM30 scoring matrices. We constructed the

767 phylogenetic tree of PilY1 sequences using a Jukes-Cantor maximum likelihood method to

768 estimate the number of substitutions between two sequences and an Unweighted Pair Group

769 Method Average (UPGMA) to construct the phylogenetic tree from the pairwise distances. 129

770 sequences of PilY1 belong to a clade with highly similar proteins, which includes PilY1 from

771 PA14. 723 sequences belong to a diverse clade that includes PilY1 from PAO1 and IPCD-83.

772 Within each of these two groups, we calculated the Shannon diversity in each position along the

773 aligned amino acid sequence using  $H = -\sum p_i \ln(p_i)$ , where  $p_i$  is the probability of each amino

774 acid (including gaps). Code is available at [github.com/GeiselBiofilm](https://github.com/GeiselBiofilm).

775

776 **Growth assays.** Overnight cultures were inoculated in M8 salts/supplements at a starting OD<sub>600</sub>  
777 of ~0.05. Readings were taken every 40 mins for 16 h in a Synergy Neo2-multimode microplate  
778 reader at the BioMT Core at the Geisel School of Medicine at Dartmouth.

779  
780 **Cloning and protein expression of GST-vWA fusions.** The coding region of the WT and the  
781 C152S mutant of the vWA domain (amino acids 30-369) from *P. aeruginosa* PA14-UCBPP were  
782 PCR amplified and cloned into pGEX-6p-1 plasmid at the BamHI cut site by Gibson assembly.  
783 *E. coli* BL21 (DE3) competent cells were transformed with plasmid and selected on LB plates  
784 with 50 µg/mL carbenicillin grown at 30 °C overnight. A single colony was used to inoculate 5  
785 mL of liquid LB and grown for 12-14 h at 30 °C. Each 5 mL seed culture was used to inoculate  
786 500 mL LB in a 2 L flask and allowed to grow at 37 °C with shaking 200 rpm until the OD<sub>600</sub> was  
787 0.6-0.8. A total of 6 L LB (12 flasks) were inoculated. Expression was induced with 0.1mM  
788 isopropylβ-D-1-thiogalactopyranoside (IPTG) for 4 h at 37 °C. Bacteria were harvested at 5,000  
789 × *g* for 10 min, washed with PBS buffer and stored at -20 °C until further use.

790  
791 **Purification of wild-type GST-vWA and Cys152S mutant proteins.** *E. coli* cells expressing  
792 WT GST-vWA and GST-vWA-C152S mutant proteins were resuspended in PBS supplemented  
793 with 2 mM TCEP (Thermo scientific), 0.01 mg/mL lysozyme from chicken egg (SIGMA), EDTA-  
794 free protease inhibitors cocktail (Blmake) and 10U/mL benzonase nuclease (Millipore) and lysed  
795 in a Microfluidizer LM10 (Microfluidics) at 18,000 psi. Nucleic acids were precipitated by addition  
796 of 0.1% polyethylenimine branched (SIGMA). Crude cell lysates were cleared by centrifugation  
797 at 200,000 × *g* for 1 hour at 4 °C in a Beckman Optima L-70 ultracentrifuge. Clear lysates were  
798 incubated overnight with 5 mL Glutathione Sepharose 4B resin (Cytiva) previously equilibrated  
799 with PBS containing 2 mM TCEP. Lysates and resin were transferred to a disposable plastic  
800 column and allowed to drain fully (flow through). Resin was washed with at least 15 column  
801 volumes of PBS, 2 mM TCEP buffer before elution of the GST-vWA proteins with 5 column

802 volumes of freshly prepared elution buffer 50 mM Tris -HCl pH 8, 10 mM reduced glutathione.  
803 Elution fractions were concentrated using 30,000 MWCO 15 mL Amicon centrifugal filters  
804 (Millipore) in a Beckman Allegra 6R centrifuge. Proteins were loaded in a HiLoad Superdex 75  
805 pg (Cytiva) pre-packed column equilibrated with 50 mM Tris-HCl pH 8, 150 mM NaCl, 1 mM  
806 TCEP using an AKTApure instrument (Cytiva). Fractions containing the fusion GST-vWA protein  
807 were combined and concentrated as before and subjected to a second gel filtration step using a  
808 high-resolution Superdex 200 increase 10/300 (Cytiva). Purified WT and C152S mutant GST-  
809 vWA proteins were extensively dialyzed against 20 mM sodium phosphate pH 7.4 buffer Final  
810 protein concentrations were determined using Bio-Rad protein assay reagent.

811 **Circular Dichroism (CD) and melting curves.** The far-UV circular dichroism (CD) spectra  
812 (195–250 nm) were recorded with a JASCO J-815 spectrophotometer (Jasco, Inc.) equipped  
813 with a CDF426S/15 Peltier temperature controller using a 2-mm path length quartz cuvette. CD  
814 spectra of proteins were recorded at 20 °C using a step size of 0.1 nm. A time constant of 12 s  
815 was used to improve the signal to noise ratio and to decrease the contribution of the solvent at  
816 lower wavelengths. CD spectra were recorded using 1 μM of GST-vWA WT and GST-vWA-  
817 C152S proteins in 20 mM sodium phosphate buffer, pH 7.4, and corrected by subtracting the  
818 spectrum of the buffer alone.

819 Thermal unfolding curves were obtained by monitoring the ellipticity at 222 and 208 nm  
820 of both fusion proteins at 1 μM concentration at a heating rate of 1 °C min<sup>-1</sup> in the temperature  
821 range of 20 to 90 °C. A 1s integration time and 5s equilibration time were used for each  
822 measurement and buffer ellipticities at the selected wavelengths were subtracted from the  
823 samples data. Raw CD data were converted into the molar ellipticity  $[\theta]_{\lambda}$  (deg cm<sup>2</sup> dmol<sup>-1</sup>) at  
824 each wavelength using the relation,  $[\theta]_{\lambda} = \theta_{\lambda}/(10CNl)$ , where  $\theta_{\lambda}$  is the observed ellipticity in  
825 millidegrees at wavelength  $\lambda$ ,  $C$  is the molar protein concentration,  $N$  is the number of amino  
826 acids of the protein, and  $l$  is the path length of the cuvette in cm. Following CD measurements,  
827 protein samples were collected, and protein concentrations measured for accuracy.

828  
829 **Acknowledgments.** We thank Roger Levesque for providing the IPCD strains used in this  
830 report and Dr. Sherry Kuchma for building the  $\Delta vWA_p$  strain. Also, thanks to Dr. Matt Wolfgang  
831 for the PilY1 antibody, Emilie Shipman for help with protein purification, Dr. Paul Delfino for  
832 technical assistance with CD, Kelsie Leary, Dr. Dean Madden and Dr. Holger Sondermann for  
833 advice on analyzing the CD data. The authors would also like to thank rotation students who  
834 worked on the project: Alexander Pastora and Rebecca Valls, other members of the O'Toole  
835 lab: Chris Geiger, Dr. Sherry Kuchma and Fabrice Jean-Pierre for helpful discussions. This work  
836 was supported by the NIH via awards R37 AI83256 (to G.A.O.), R01 AI43730 (to G.C.L.W.) and  
837 COBRE/NIGMS 5 P20 GM130454-02 (to D.S). This work was also supported by bioMT through  
838 NIH NIGMS grant P20-GM113132. Work at UCLouvain was supported by the Excellence of  
839 Science-EOS programme (Grant #30550343), the European Research Council (ERC) under the  
840 European Union's Horizon 2020 research and innovation programme (grant agreement  
841 n°693630), and the National Fund for Scientific Research (FNRS). Y.D. is a Research Director  
842 at the FNRS.

843  
844  
845 **References**

- 846  
847 1. Ellison, C.K., et al., *Obstruction of pilus retraction stimulates bacterial surface sensing*. Science,  
848 2017. **358**(6362): p. 535-538.  
849 2. Persat, A., et al., *Type IV pili mechanochemically regulate virulence factors in Pseudomonas*  
850 *aeruginosa*. Proc Natl Acad Sci U S A, 2015. **112**(24): p. 7563-8.  
851 3. Luo, Y., et al., *A hierarchical cascade of second messengers regulates Pseudomonas aeruginosa*  
852 *surface behaviors*. mBio, 2015. **6**(1).  
853 4. Siryaporn, A., et al., *Surface attachment induces Pseudomonas aeruginosa virulence*. Proc Natl  
854 Acad Sci U S A, 2014. **111**(47): p. 16860-5.  
855 5. Treuner-Lange, A., et al., *PilY1 and minor pilins form a complex priming the type IVa pilus in*  
856 *Myxococcus xanthus*. Nat Commun, 2020. **11**(1): p. 5054.  
857 6. Nguyen, Y., et al., *Pseudomonas aeruginosa minor pilins prime type IVa pilus assembly and*  
858 *promote surface display of the PilY1 adhesin*. J Biol Chem, 2015. **290**(1): p. 601-11.  
859 7. Rossmann, M.G., D. Moras, and K.W. Olsen, *Chemical and biological evolution of nucleotide-*  
860 *binding protein*. Nature, 1974. **250**(463): p. 194-9.  
861 8. Lee, J.O., et al., *Crystal structure of the A domain from the alpha subunit of integrin CR3*  
862 *(CD11b/CD18)*. Cell, 1995. **80**(4): p. 631-8.

- 863 9. Konto-Ghiorgi, Y., et al., *Dual role for pilus in adherence to epithelial cells and biofilm formation*  
864 *in Streptococcus agalactiae*. PLoS Pathog, 2009. **5**(5): p. e1000422.
- 865 10. Raynaud, C., et al., *PilB from Streptococcus sanguinis is a bimodular type IV pilin with a direct*  
866 *role in adhesion*. Proc Natl Acad Sci U S A, 2021. **118**(22).
- 867 11. Shapiro, S.E., et al., *The von Willebrand factor predicted unpaired cysteines are essential for*  
868 *secretion*. J Thromb Haemost, 2014. **12**(2): p. 246-54.
- 869 12. Schneider, S.W., et al., *Shear-induced unfolding triggers adhesion of von Willebrand factor fibers*.  
870 Proc Natl Acad Sci U S A, 2007. **104**(19): p. 7899-903.
- 871 13. Zhang, Q., et al., *Structural specializations of A2, a force-sensing domain in the ultralarge*  
872 *vascular protein von Willebrand factor*. Proc Natl Acad Sci U S A, 2009. **106**(23): p. 9226-31.
- 873 14. Aponte-Santamaria, C., et al., *Force-sensitive autoinhibition of the von Willebrand factor is*  
874 *mediated by interdomain interactions*. Biophys J, 2015. **108**(9): p. 2312-21.
- 875 15. Gogia, S. and S. Neelamegham, *Role of fluid shear stress in regulating VWF structure, function*  
876 *and related blood disorders*. Biorheology, 2015. **52**(5-6): p. 319-35.
- 877 16. Purvis, A.R., et al., *Two Cys residues essential for von Willebrand factor multimer assembly in the*  
878 *Golgi*. Proc Natl Acad Sci U S A, 2007. **104**(40): p. 15647-52.
- 879 17. Rodesney, C.A., et al., *Mechanosensing of shear by Pseudomonas aeruginosa leads to increased*  
880 *levels of the cyclic-di-GMP signal initiating biofilm development*. Proc Natl Acad Sci U S A, 2017.  
881 **114**(23): p. 5906-5911.
- 882 18. Kuchma, S.L., et al., *Cyclic-di-GMP-mediated repression of swarming motility by Pseudomonas*  
883 *aeruginosa: the pilY1 gene and its impact on surface-associated behaviors*. J Bacteriol, 2010.  
884 **192**(12): p. 2950-64.
- 885 19. Cady, K.C., et al., *The CRISPR/Cas adaptive immune system of Pseudomonas aeruginosa*  
886 *mediates resistance to naturally occurring and engineered phages*. J Bacteriol, 2012. **194**(21): p.  
887 5728-38.
- 888 20. Webster, S.S., et al., *Interaction between the type 4 pili machinery and a diguanylate cyclase*  
889 *fine-tune c-di-GMP levels during early biofilm formation*. Proc Natl Acad Sci U S A, 2021. **118**(26).
- 890 21. Butera, D., et al., *Autoregulation of von Willebrand factor function by a disulfide bond switch*. Sci  
891 Adv, 2018. **4**(2): p. eaaq1477.
- 892 22. Ganderton, T., et al., *Lateral self-association of VWF involves the Cys2431-Cys2453*  
893 *disulfide/dithiol in the C2 domain*. Blood, 2011. **118**(19): p. 5312-8.
- 894 23. Tripathi, P., et al., *Adhesion and nanomechanics of pili from the probiotic Lactobacillus*  
895 *rhamnosus GG*. ACS Nano, 2013. **7**(4): p. 3685-97.
- 896 24. Mignolet, J., et al., *AFM Unravels the Unique Adhesion Properties of the Caulobacter Type IVc*  
897 *Pilus Nanomachine*. Nano Lett, 2021. **21**(7): p. 3075-3082.
- 898 25. Beaussart, A., et al., *Nanoscale adhesion forces of Pseudomonas aeruginosa type IV Pili*. ACS  
899 Nano, 2014. **8**(10): p. 10723-33.
- 900 26. Freschi, L., et al., *Clinical utilization of genomics data produced by the international*  
901 *Pseudomonas aeruginosa consortium*. Front Microbiol, 2015. **6**: p. 1036.
- 902 27. Freundt, J.K. and W.A. Linke, *Titin as a force-generating muscle protein under regulatory control*.  
903 J Appl Physiol (1985), 2019. **126**(5): p. 1474-1482.
- 904 28. Eckels, E.C., et al., *The Work of Titin Protein Folding as a Major Driver in Muscle Contraction*.  
905 Annu Rev Physiol, 2018. **80**: p. 327-351.
- 906 29. Marszalek, P.E., et al., *Mechanical unfolding intermediates in titin modules*. Nature, 1999.  
907 **402**(6757): p. 100-3.
- 908 30. Rack, K., et al., *Margination and stretching of von Willebrand factor in the blood stream enable*  
909 *adhesion*. Sci Rep, 2017. **7**(1): p. 14278.

- 910 31. Sadler, J.E., *Biochemistry and genetics of von Willebrand factor*. Annu Rev Biochem, 1998. **67**: p.  
911 395-424.
- 912 32. Giganti, D., et al., *Disulfide isomerization reactions in titin immunoglobulin domains enable a*  
913 *mode of protein elasticity*. Nat Commun, 2018. **9**(1): p. 185.
- 914 33. Marti, T., et al., *Identification of disulfide-bridged substructures within human von Willebrand*  
915 *factor*. Biochemistry, 1987. **26**(25): p. 8099-109.
- 916 34. Eckels, E.C., et al., *The Mechanical Power of Titin Folding*. Cell Rep, 2019. **27**(6): p. 1836-1847 e4.
- 917 35. Jones, C.H., et al., *FimH adhesin of type 1 pili is assembled into a fibrillar tip structure in the*  
918 *Enterobacteriaceae*. Proc Natl Acad Sci U S A, 1995. **92**(6): p. 2081-5.
- 919 36. Nilsson, L.M., et al., *The cysteine bond in the Escherichia coli FimH adhesin is critical for adhesion*  
920 *under flow conditions*. Mol Microbiol, 2007. **65**(5): p. 1158-69.
- 921 37. Dufrene, Y.F., et al., *AFM in cellular and molecular microbiology*. Cell Microbiol, 2021. **23**(7): p.  
922 e13324.
- 923 38. Armbruster, C.R., et al., *Heterogeneity in surface sensing suggests a division of labor in*  
924 *Pseudomonas aeruginosa populations*. Elife, 2019. **8**.
- 925 39. Lee, C.K., et al., *Multigenerational memory and adaptive adhesion in early bacterial biofilm*  
926 *communities*. Proc Natl Acad Sci U S A, 2018. **115**(17): p. 4471-4476.
- 927 40. Kulasekara, B.R., et al., *c-di-GMP heterogeneity is generated by the chemotaxis machinery to*  
928 *regulate flagellar motility*. Elife, 2013. **2**: p. e01402.
- 929 41. Skerker, J.M. and H.C. Berg, *Direct observation of extension and retraction of type IV pili*. Proc  
930 Natl Acad Sci U S A, 2001. **98**(12): p. 6901-4.
- 931 42. Cowles, K.N. and Z. Gitai, *Surface association and the MreB cytoskeleton regulate pilus*  
932 *production, localization and function in Pseudomonas aeruginosa*. Mol Microbiol, 2010. **76**(6): p.  
933 1411-26.
- 934 43. Kelly, N.M., et al., *Pseudomonas aeruginosa pili as ligands for nonopsonic phagocytosis by*  
935 *fibronectin-stimulated macrophages*. Infect Immun, 1989. **57**(12): p. 3841-5.
- 936 44. Speert, D.P., et al., *Nonopsonic phagocytosis of nonmucoid Pseudomonas aeruginosa by human*  
937 *neutrophils and monocyte-derived macrophages is correlated with bacterial piliation and*  
938 *hydrophobicity*. Infect Immun, 1986. **53**(1): p. 207-12.
- 939 45. Bradley, D.E., *Evidence for the retraction of Pseudomonas aeruginosa RNA phage pili*. Biochem  
940 Biophys Res Commun, 1972. **47**(1): p. 142-9.
- 941 46. Laventie, B.J., et al., *A Surface-Induced Asymmetric Program Promotes Tissue Colonization by*  
942 *Pseudomonas aeruginosa*. Cell Host Microbe, 2019. **25**(1): p. 140-152 e6.
- 943 47. Shanks, R.M., et al., *Saccharomyces cerevisiae-based molecular tool kit for manipulation of*  
944 *genes from gram-negative bacteria*. Appl Environ Microbiol, 2006. **72**(7): p. 5027-36.
- 945 48. Silayeva, O. and A.C. Barnes, *Gibson Assembly facilitates bacterial allelic exchange mutagenesis*.  
946 J Microbiol Methods, 2018. **144**: p. 157-163.
- 947 49. Bachman, J., *Site-directed mutagenesis*. Methods Enzymol, 2013. **529**: p. 241-8.
- 948 50. O'Toole, G.A. and R. Kolter, *Flagellar and twitching motility are necessary for Pseudomonas*  
949 *aeruginosa biofilm development*. Mol Microbiol, 1998. **30**(2): p. 295-304.
- 950 51. O'Toole, G.A., *Microtiter dish biofilm formation assay*. J Vis Exp, 2011(47).
- 951 52. Bradford, M.M., *A rapid and sensitive method for the quantitation of microgram quantities of*  
952 *protein utilizing the principle of protein-dye binding*. Anal Biochem, 1976. **72**: p. 248-54.
- 953 53. Li, L., et al., *Charge Calibration Standard for Atomic Force Microscope Tips in Liquids*. Langmuir,  
954 2020. **36**(45): p. 13621-13632.

955